Int. J. Electrochem. Sci., 15 **(2020)** 442 – 457, doi: 10.20964/2020.01.01

International Journal of
ELECTROCHEMICAL
SCIENCE
www.electrochemsci.org

The Application of Zinc Oxide Nanoparticles as An Eco-Friendly Inhibitor for Steel in Acidic Solution

Reema H. Al-Dahiri[1], *Aisha M. Turkustani*[1,2], *Mohamed Abdel Salam*[1]

[1] Chemistry Department, Faculty of Science for Girls, King Abdulaziz University, P.O. Box 80200, Jeddah 21589, Saudi Arabia.
[2] Chemistry Department, Faculty of Science for Girls, Jeddah University, Jeddah, Saudi Arabia
*E-mail: masalam16@hotmail.com

Received: 1 September 2019 / *Accepted:* 23 October 2019 / *Published:* 30 November 2019

In this study, zinc oxide nanoparticles were prepared using a natural extract of Myrrh as green capping agent. The synthesized ZnO-NPs (Zinc Oxide Nanoparticles) were characterized using XRD and scanning electron microscopy, and the results revealed the synthesis of hexagonal wurtzite ZnO-NPs. The corrosion inhibition of steel in 1.0 M HCl using an aqueous extract of natural Myrrh and the green-synthesized ZnO-NPs was investigated at various concentrations using electrochemical impedance spectroscopy (EIS) measurements and potentiodynamic polarization (PDP). The results revealed that the corrosion inhibition process is exponentially increased with the inhibitor concentrations, and an inhibition effectiveness of 92% could be acquired. Polarization curves showed that the eco-friendly inhibitors perform as a cathodic inhibitor. Consequently, the obtained inhibition efficiency values derived from all chosen analysis techniques were in reasonably good agreement.

Keywords: corrosion; steel, *Myrrh*, green synthesis, zinc oxide nanoparticles

1. INTRODUCTION

In recent years, nanotechnology has become one of the fastest growing technologies in the world due to significant improvements in the physical, chemical, optical, and mechanical properties of matter reduced to a nanometer size. Accordingly, a significant amount of research has been performed in different fields [1-6]. Zinc oxide nanoparticles (ZnO-NPs) are among the most frequently used semiconductors in nanotechnology and are characterized by their large excitation binding energy (60 meV) and wide band gap (3.37 eV) in addition to their unique electrical, optical, catalytic, and photochemical properties [7]. The advantages of ZnO-NPs over other NPs include their applications in the fields of environmental treatment [8, 9] and corrosion protection [10-14].

Corrosion is a destructive phenomenon, and inhibiting this process is essential in terms of cost and security, especially for metals. Corrosion is unavoidable but can be controlled via metal dissolution, which reduces the corrosion rate [15] through various mechanisms, such as a metal coating [16], a cathodic protection process [17], and inhibition [18]. Specifically, inhibitors are the most common method used for corrosion protection due to their easy application to different technical sections as well as their high efficiency [19, 20]. Organic-based chemical compounds containing aromatic rings, multiple bonds, or active atoms such as oxygen, sulfur, and nitrogen are usually used as inhibitors due to their highly efficient ability to inhibit metal corrosion; they are, however, quite expensive and can cause more adverse effects and potential environmental pollution. Accordingly, scientists throughout the world have been devoted to searching for natural corrosion inhibitors, such as green plant extracts (e.g., seeds, leaves, flowers, and fruits) and natural polysaccharides; they are a rich source of natural chemical compounds as well as being inexpensive, eco-friendly, renewable, and biodegradable, especially when compared to those of organic-based chemical inhibitors [21-38]. In recent years, several studies have analyzed plant biomaterials as metal corrosion inhibitors in different corrosive media.

The inhibition mechanism of the metals by green inhibitors in different corrosive media is mainly due to the adsorption of green inhibitor molecules on the surface of the metal, which block the metal surfaces and prevent the corrosion process [36-42].

Myrrh resin is a solid natural gum extracted from a small tree species of the genus *Commiphora* and is frequently used as perfume, incense, and medicine, since it contains volatile oil, alcohol-soluble resins, and water-soluble gum. The water-soluble gum contains a mixture of proteoglycans—with polymers of uronic acid—and the main natural product constituent of *Myrrh* gum are L-arabinose, 4-methyl D-glucuronic, and D-galactose acid (in a proportion of 1:3:4) [37]. *Myrrh* oil consists of many chemical compounds (Table 1), including functional groups such as amines and aldehydes, which are very effective in the inhibition of different metal surface corrosion processes [37, 43].

Table 1. Molecular structure of some components in *Myrrh*

Molecular structure of some components in *Myrrh*	Name	Molecular structure of some components in *Myrrh*	Name
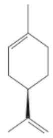	limonene	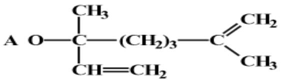 $\mathrm{A\ O{-}C(CH_3)(CH{=}CH_2){-}(CH_2)_3{-}C({=}CH_2)CH_3}$	Isolinalyl acetate

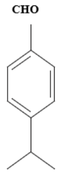	cuminaldehyde	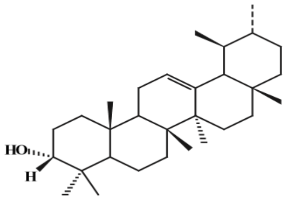	3-epi-α-amirin
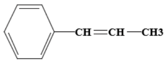	cinnamic aldehyde	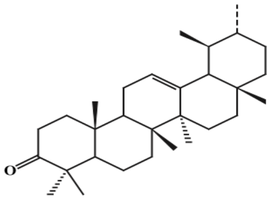	α-amirone
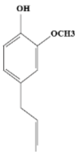	eugenol	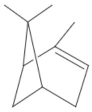	α-pinene
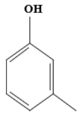	m-cresol	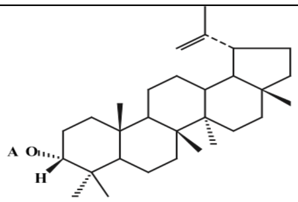	3-epi-lupenyl acetate

To continue investigating and improving the efficiency and effectiveness of corrosion inhibition, the present work focused on a green method preparation of ZnO-NPs using inexpensive, nontoxic, natural *Myrrh* gum as a new capping agent to prevent their agglomeration. This study also further investigates the application of the *Myrrh* extract and the green-prepared ZnO-NPs as inhibitors of steel corrosion in an acidic medium using electrochemical measurements.

2. EXPERIMENTAL

2.1. Chemicals and Materials

Zinc sulfate ($ZnSO_4.7H_2O$) and sodium hydroxide (NaOH) were obtained from Aldrich Chemical Co. *Myrrh* gum, which is yellowish red in color, was extracted from a tree. Aggressive solutions of 0.1 M HCl (analytical grade 37%) were prepared by diluting with distilled water. The chemical composition of the steel samples used for measurements was (wt.%) 0.15 C, 0.75 Mn, 0.015 P, 0.02 S, 0.23 Si, and iron remainder. The sample surfaces were prepared using emery paper of grade 60-1200. They were then washed with double distilled water and acetone. Finally, the sample was dried with an air stream before its immersion in the experiment solution.

2.2. Traditional Preparation of Zinc Oxide Nanoparticles

A $ZnSO_4$ solution (0.1 M) was added dropwise to a heated solution of 0.4 M NaOH (80 °C) under continuous magnetic stirring, and the produced white precipitate of $Zn(OH)_2$ was filtered, washed with distilled water three times, then with acetone, and finally left to dry overnight at room temperature. Obtaining ZnO-NPs with various morphologies was made possible by changing the different parameters of the precipitation procedure, such as the pH, washing medium, calcination temperature, or solution concentration [44]. In this study, ZnO-NPs were obtained via calcination of the white-precipitated $Zn(OH)_2$ at different temperatures (100 °C–600 °C).

2.3. Green Preparation of ZnO NPs

Zinc sulfate was dissolved in a solution of *Myrrh* extract (1 g/L) under continual stirring to prepare a 0.1 M aqueous solution. Additionally, NaOH was dissolved in the *Myrrh* extract solution (1 g/L) to prepare a 0.4 M aqueous solution. The aqueous solution of 0.1 M $ZnSO_4$ and *Myrrh* extract was dropwise added to a heated solution of the 0.4 M NaOH (80 °C) in *Myrrh* extract under continuous magnetic stirring for 60 min. Mixing was carried out until the complete precipitation of $Zn(OH)_2$. The precipitated $Zn(OH)_2$ was then filtered, washed with distilled water three times, then washed with acetone and left to dry overnight at room temperature. Finally, the dried product was calcined at different temperatures (100 °C–600 °C).

2.4. Characterization of ZnO Nanoparticles

X-ray powder diffraction (XRD) was performed for the prepared ZnO-NPs using a Bruker diffractometer (Bruker D8 advance target). XRD was run with copper $K_{\alpha 1}$ and a monochromator (λ= 1.5405A$^{\circ}$) at 40 kV and 40 mA. The SEM (Scanning Electron Microscopy) measurements for ZnO-NPs were carried out using an FESEM (Jeol JSM-7600F) system. The sample morphology and microanalysis were performed using a digital electron microscope *(magnification ratio 40x-1000x).*

2.5. Electrochemical Analysis Measurements

The two techniques of electrochemical measurement analysis (e.g., EIS and PDP) were conducted in a Pyrex cell with a total volume of 100 cm^3. The three electrodes immersed in the glass cell assembly included the aggressive solution at room temperature. The electrochemical cell consisted of three electrodes: the corrosion electrode (working electrode), the reference electrode (Ag/ AgCl, saturated KCl), and a platinum counter electrode. The potential scan rate was 5 mVs^{-1} with an impedance frequency range of 10 KHz –10 mHz. The signal amplitude perturbation = 10 mV. An Interface 1000 (Gamry Instruments, USA) potentiostat/galvanostat was used in this study to monitor the electrochemical behavior and obtain corrosion measurements.

3. RESULTS AND DISCUSSION

3.1. Characterization of ZnO NPs

Figure 1 shows the XRD patterns for the traditional ZnO-NPs (a) and the ZnO-NPs prepared by *Myrrh.* For both patterns, the characteristic peaks of the ZnO-NPs were identified from three main diffraction peaks at 2θ = 31.72, 34.38, and 36.20°, corresponding to the (100), (002), and (101) crystal planes of the hexagonal wurtzite ZnO (JCPDS file no.89-0511). Moreover, there were no extra diffraction peaks identical to Zn or other ZnO phases discovered, revealing that the traditional ZnO-NPs were crystalline in nature. The peak intensities were narrow and sharp, indicating that the sample was of high quality with good crystallinity and a fine grain size.

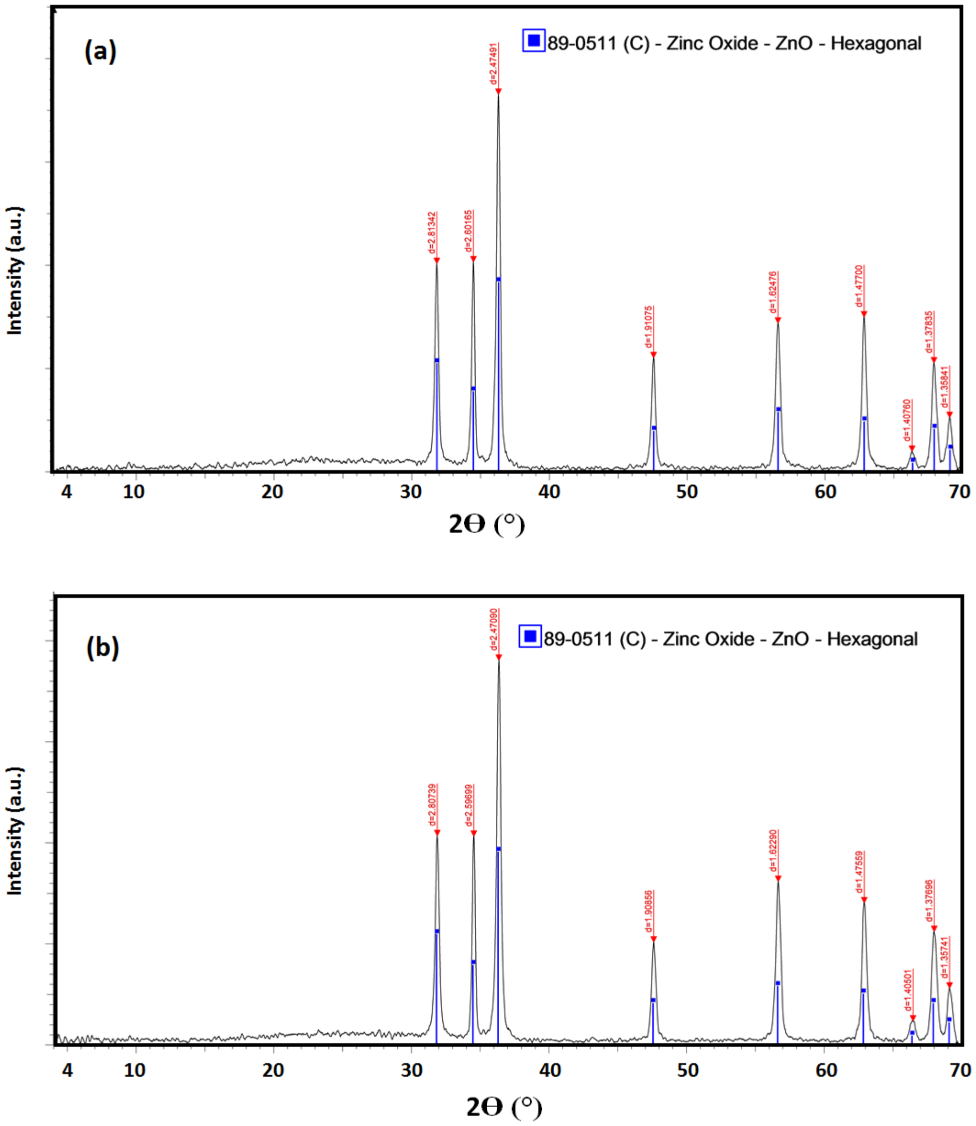

Figure 1. XRD diffraction pattern of traditional ZnO-NPs (a) and ZnO-NPs prepared by Myrrh (b).

The surface morphology of the traditional ZnO-NPs (a) and ZnO-NPs prepared by *Myrrh* was explored using an FESEM analysis (Figure 2). Traditional ZnO-NPs had an agglomerated, rod-like shape with different lengths and an average diameter of 75 nm, whereas surprisingly, ZnO-NPs prepared by *Myrrh* were agglomerated spherical-like particles with an average diameter of 75 nm. This may indicate the role of *Myrrh* as a natural capping agent that prevents the agglomeration and formation of a rod-like shape similar to that produced by the traditional preparation method.

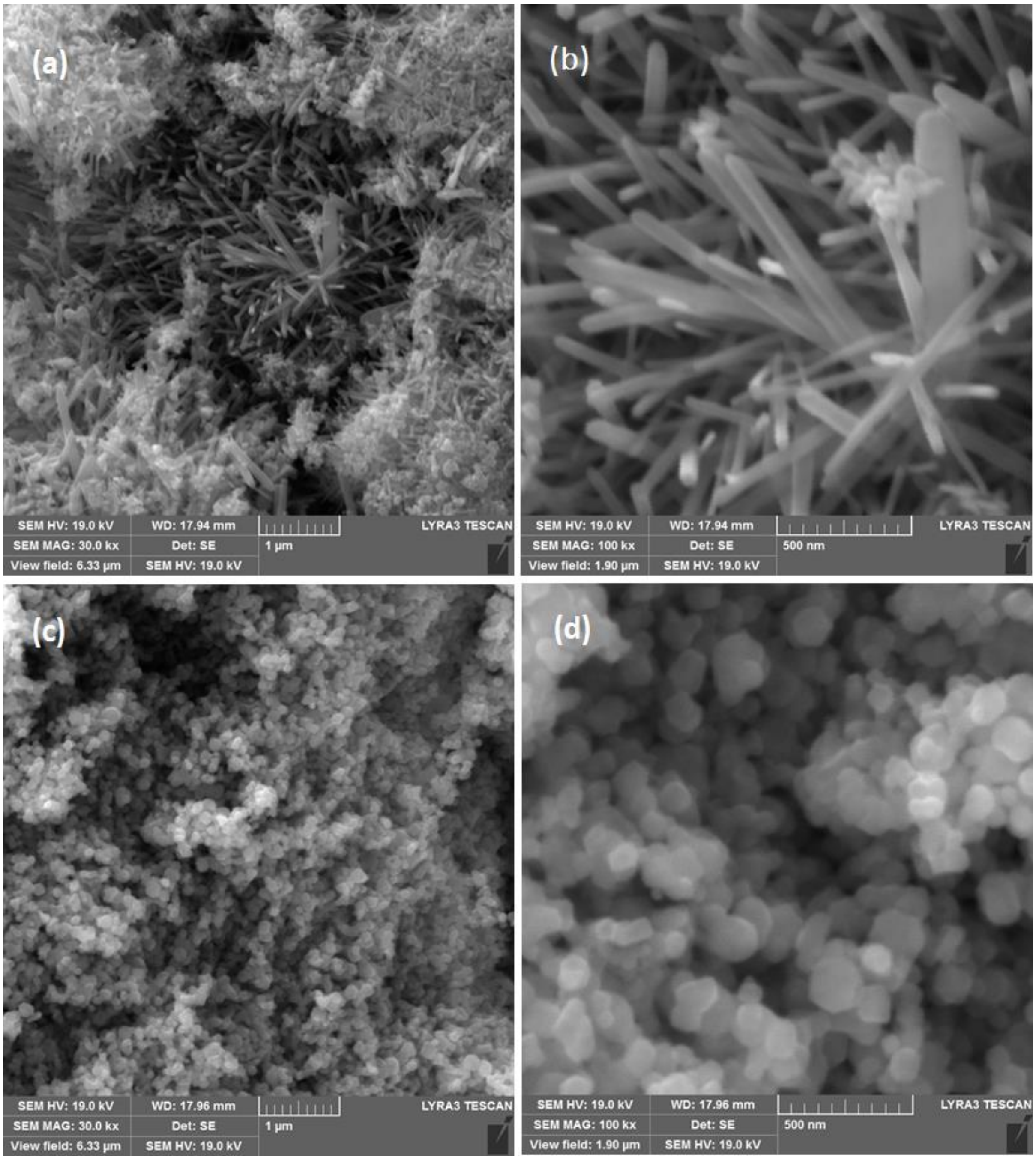

Figure 2. SEM images of traditional ZnO-NPs (a, b) and green ZnO-NPs prepared by Myrrh (c, d), at different magnification powers.

3.2. Potentiodynamic Polarization Measurements

Tafel curves were constructed to study the kinetics of the reduction and oxidation reactions of steel dissolution in a 1.0 M HCl acid solution in the absence and presence of *Myrrh* (Figure 3). Figure 4 shows the effect of the absence and presence of ZnO-NPs. These figures reveal that the presence of the *Myrrh* extract and/or ZnO-NPs leads to a decrease in dissolution currents and the hydrogen evolution process. The reduction was more significant for the cathodic curves than for the anodic curve. The polarization parameters of the *Myrrh*—such as corrosion potential (E_{corr}), cathodic and anodic Tafel slopes (b_a and b_c), and the current density of corrosion (I_{corr}), which were acquired via the extrapolation of the Tafel slopes—are recorded in Table 2, while the same corrosion parameters for ZnO-NPs are listed in Table 3. It is clear from these tables that increasing the additive concentration decreases I_{corr}. The results also suggest that *Myrrh* and/or ZnO-NPs work as mixed type mainly cathodic inhibitors, since the majority of the cathodic reaction is more effective than that of the anodic reaction [44]. Corrosion potential (E_{corr}) was observed to move against more negative potentials with increasing inhibitor concentrations, suggesting the inhibitors were of mainly a cathodic character. Hence, the presence of *Myrrh* and ZnO-NPs in an aggressive acidic solution prevents both reactions with a total shift of E_{corr} to more negative values than that from the blank solution.

Table 2. Electrochemical parameters and inhibition efficiency values for steel in 1.0 M HCl at different concentrations of *Myrrh* calculated by *PDP* and *EIS* methods at *30 ˚C*

	Method			**PDP**				**EIS**	
$C_{inh.}$ (g/l)	$b_a \times 10^{-3}$ (mV. dec^{-1})	$b_c \times 10^{-3}$ (mV. dec^{-1})	$-E_{corr}$ (mV)	i_{corr} (μA)	R_{corr} (mV)	IE%	R_{ct} Ωcm^2	$Cdl \times 10^{-6}$ (μF/cm)	IE%
Blank	88	67	413	800	364	-----	16.20	998	-----
0.0025	138	111	431	550	242	31.25	26.52	695	38.91
0.0050	140	122	439	382	228	52.25	38.20	511	58.43
0.0100	153	136	506	349	165	56.38	43.43	401	62.70
0.0150	153	140	523	271	144	66.13	67.27	307	75.92
0.0200	154	156	530	205	117	74.38	84.37	211	80.80

Table 3. Electrochemical parameters and inhibition efficiency values for steel in 1.0 M HCl at different concentrations of ZnO-NPs calculated by *PDP* and *EIS* methods at *30 ˚C*

	Method			**PDP**				**EIS**	
$C_{inh.}$ (g/l)	$b_a \times 10^{-3}$ (mV. dec^{-1})	$b_c \times 10^{-3}$ (mV. dec^{-1})	$-E_{corr}$ (mV)	i_{corr} (μA)	R_{corr} (mV)	IE%	R_{ct} Ωcm^2	$Cdl \times 10^{-6}$ (μF/cm)	IE%
Blank	88	67	413	800	364	-----	16.20	998	-----
0.0025	146	99	531	243	1886	69.63	63.32	313	74.43
0.0050	162	107	532	230	139	71.25	79.20	288	79.55
0.0100	175	117	536	162	123	79.75	126.6	204	87.20
0.0150	179	117	541	133	109	83.38	158.6	131	89.79
0.0200	183	120	542	81	96	89.88	209.1	100	92.25

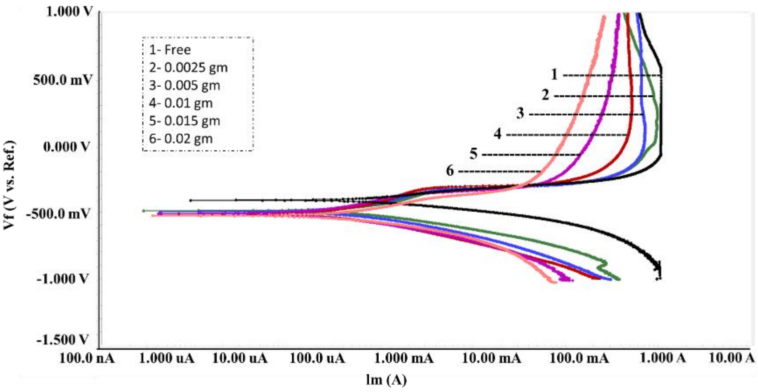

Figure 3. Potentiodynamic polarization curves for steel in 1.0 M HCl solution at various concentrations of Myrrh at 30 °C. [Scan Rate: 5mV, Initial E: -0.5 V, Final E: 2V]

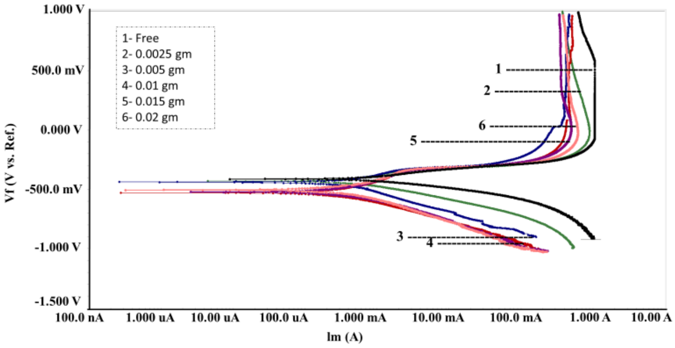

Figure 4. Potentiodynamic polarization curves for steel in 1.0 M HCl solution at various concentrations of ZnO-NPs at 30 °C. [Scan Rate: 5mV, Initial E: -0.5 V, Final E: 2V]

The inhibition efficiency (IE%) was calculated from the I_{corr} values using the following equation [45]:

$$IE_{Icoor}\% = 1 – I_{corr\,(inh)} / I_{corr} \text{ x } 100 \qquad (1)$$

where I_{corr} and $I_{corr\,(inh)}$ are the corrosion current densities in the absence and presence of additives, respectively. The inhibition efficiency values at various concentrations of *Myrrh* and/or ZnO-NPs are recorded in Tables 2 and 3. Given the values of the protection efficiency in Tables 2 and 3, *Myrrh* and ZnO-NPs both act as effective corrosion protection for steel in a 1.0 M HCl acid solution. Furthermore, the inhibition efficiency increased as the concentration of inhibitor increased. Additionally, the higher value of inhibition efficiency found with ZnO-NPs than that of *Myrrh* without ZnO-NPs can be attributed to a synergistic effect with ZnO-NPs, which increases the adsorption of more inhibitor molecules on the steel surface as well as increases the PE%. The modified surface with high cover action would then be enhanced by the formation of a cohesive layer of ZnO-NPs over the entire surface. This layer prevents the underlying substrate from corrosion as the plate becomes exposed to the aggressive medium. The results indicate the small size of the ZnO nanoparticles, which increased the adsorption surface area on the steel surface.

3.3 EIS Measurement

Figures 5 and 6 show Nyquist plots for the steel sample in a 1.0 M HCl solution in the absence and presence of different concentrations of *Myrrh* and/or ZnO-NPs, respectively. A capacitive loop corresponds to the semicircle in various concentrations in all cases. It was also observed that the diameter of the capacitive loop increases within increasing concentrations. To establish a good fit to the experimental data and identify the impedance parameters of steel in 1 M HCl, an equivalent circuit (EC) (Figure 7) was used. Extract data were judged by a chi-square (χ^2) test, which was approximately 10^{-3}–10^{-6}. The circuit consisted of R_s (solution resistance), R_{ct} (charge transfer resistance), and C_{dl} (double layer capacitance). From the results of the electrochemical impedance spectroscopy data, it could be observed that the corrosion of the steel sample in 1.0 M HCl was controlled by a charge transfer process. Tables 2 and 3, list the parameters obtained from the impedance of *Myrrh* and/or Zinc Oxide Nanocomposite, respectively, by fitting the EIS data to the equivalent circuit. In addition, it should be noted that the charge transfer resistance rapidly increased with additive concentration. Furthermore, the capacitance values decreased, suggesting the formation of a protective film on the steel surface. The slower corroding system was associated with high R_{ct} values [46-48]. There were also two factors that enhanced the decrease in C_{dl}: (1) a decrease in the dielectric constant or (2) an increase in the electrical double layer thickness [45]. In this regard, the reduction in C_{dl} values and the expansion of the R_{ct} values can be accounted for by the progressive substitution of H_2O molecules with the inhibitor particles adsorbed on the metal surface. The inhibition efficiency (IE_{Rct}%) was calculated from the R_{ct} values using the following equation:

$$IE_{Rct}\% = 1 - R_{1ct}/R_{2ct} \times 100 \quad (2)$$

where R_{1ct} is the resistance of the charge transfer in the absence of additives and R_{2ct} is the resistance of the charge transfer in the absence of the inhibitor.

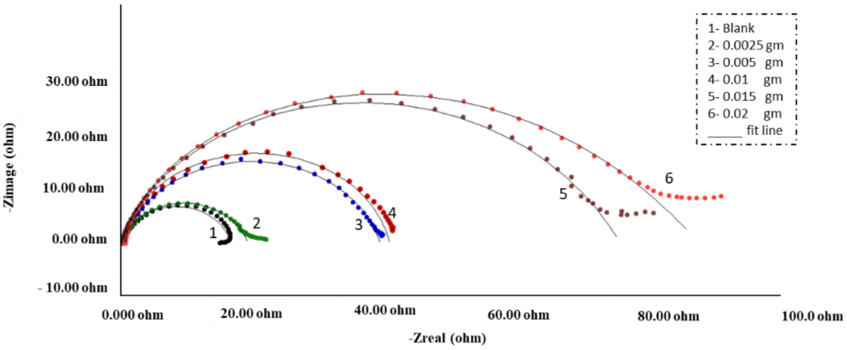

Figure 5. Nyquist plots for steel in 1.0 M HCl solution at various concentrations of Myrrh at 30 °C. [Frequency: 100,000-0.1 Hz, AC Voltage: 10 mV rms, Estimated Z: 100 ohms]

The IE% values at various concentrations of additives are listed for both *Myrrh* and ZnO NPs in Tables 2 and 3, respectively. In the case of ZnO-NPs, the efficiency of inhibition was attributed to the size of the nanoparticles, which have the ability to penetrate the surface of the metal, thus, locking active centers on the surface. The higher values of IE% with the addition of green-synthesized ZnO-NPs by *Myrrh* can be assigned to an increase in the inhibitor adsorption with the formation of a homogeneous film on the steel surface. This uniform film enhanced the adsorption (interaction) of the inhibitor molecule on the steel surface in the presence of the zinc oxide nanocomposite. In conclusion, there is strong agreement of the inhibition efficiency results, which were calculated using two electrochemical measurements (e.g., PDP and EIS) [44].

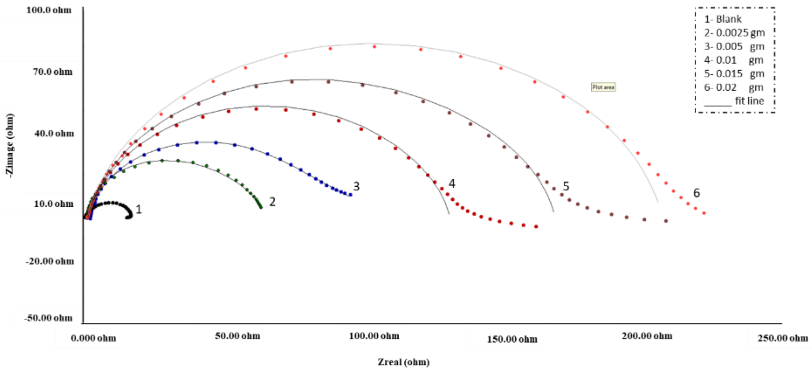

Figure 6. Nyquist plots for steel in 1.0 M HCl solution at various concentrations of ZnO-NPs at 30 °C.[Frequency: 100,000-0.1 Hz, AC Voltage: 10 mV rms, Estimated Z: 100 ohms]

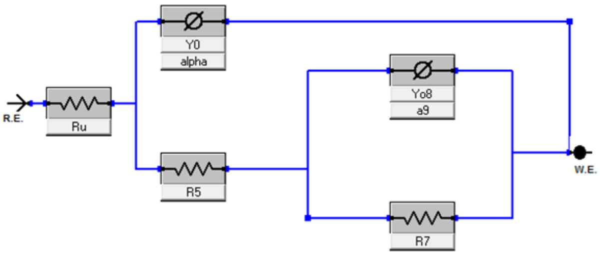

Figure 7. Electrochemical equivalent circuit.

3.4 Adsorption Isotherm and Inhibition Mechanism

The relationship between the interface coverage of the adsorbed species and the species concentration in the solution can be called an adsorption isotherm, which highlights the basic function of the interaction between the ZnO-NP inhibitor and the steel surface. This relationship is specifically between the surface coverage degree (θ) values and the inhibitor concentrations (C) in the HCl solution, which were produced from measurements of polarization and impedance. The relationship between the (θ) values and the different *Myrrh* and/or ZnO-NP concentrations is presented in Figure 8. Figure 8a, which shows a curve with two *S*-shapes, illustrates that the adsorption of *Myrrh* on the steel surface occurs in two steps, both of which enhance adsorption and inhibition. Furthermore, Figure 8b also shows an *S*-shaped adsorption isotherm, indicating the formation of a monolayer adsorbate film on the steel surface. To obtain the best fit for the adsorption, the values of (θ) can be used in different equations by examining the isotherm data at a certain temperature.

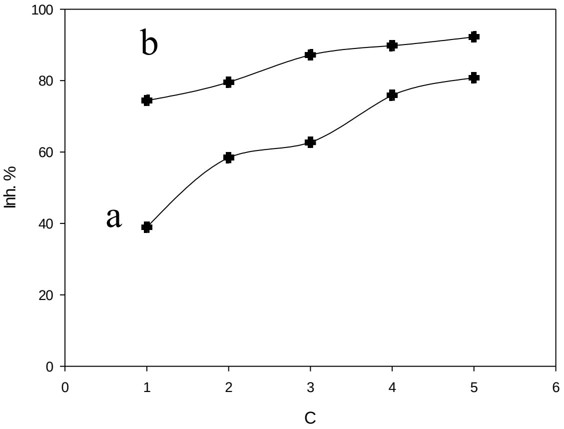

Figure 8. The relationship between inhibitor concentrations. (a) Myrrh (b) ZnO-NPs/Myrrh and the inhibition efficiencies to fit the impedance spectra at 30 °C.

To identify the interaction between the ZnO-NP molecules and the steel surface in the HCl solution, one or more of the Freundlich, Frumkin, Flory-Huggins, Langmuir, and Temkin adsorption isotherms can be used. In this study, the best fit for the experimental data was achieved by applying the Langmuir model (Eq. (3)) [49, 50] with the highest regression factor (R_2). An $R_2>0.9999$ correlation coefficient of the straight line suggests that the adsorption followed the Langmuir adsorption isotherm.

$$C/\theta = 1/K_{ads} + C \qquad (3)$$

As illustrated in Figure 9, the Langmuir plots drawn between the (θ) data from the EIS analysis and PDP measurements show that increasing concentration increases corrosion inhibition. Furthermore, from the isotherm, the Gibbs free energy (ΔG_{ads}) can be deduced using the following expression [16, 51]:

$$\Delta G_{ads} = -RT \ln (10^6 K_{ads}) \qquad (4)$$

Values corresponding to the change in free energy adsorption (ΔG_{ads}) were calculated and are listed in Table 4. The values of ΔG_{ads} obtained from the PDP and EIS techniques were -32.22 kJ mol^{-1} and -33.18 kJ mol^{-1}, respectively. The negative sign for the ΔG_{ads} value indicates that the ZnO-NP species are spontaneously adsorbed on the steel surface [52]. Furthermore, the ΔG_{ads} value indicates that this adsorption is physical and confirms the experimental details.

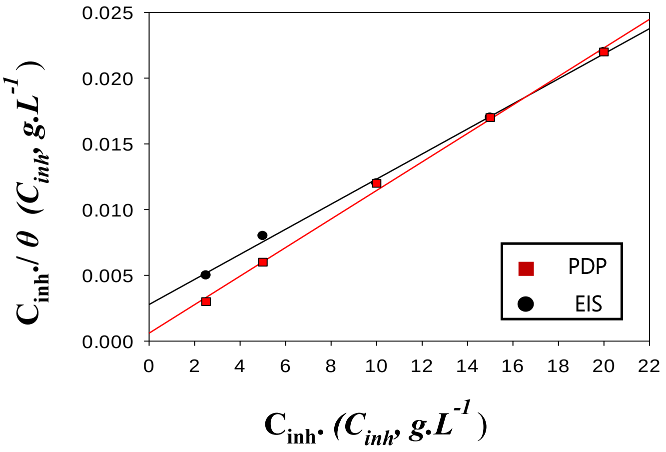

Figure 9. Fitting of θ values at different concentrations of ZnO-NPs by the Langmuir adsorption isotherm model.

Table 4. Isotherm parameters for ZnO-NPs on the steel surface in 1.0 M HCl estimated from the Langmuir model.

Adsorption isotherm model	**Method**	
	PDP	**EIS**
K_L (L.g^{-1})	0.359	0.524
slope	1.085	0.954
r^2	0.99	0.95
ΔG_{ads}	-32	-33

3.5 Mechanism

There are different ways to adsorb the inhibitors molecules on the metal/solution interface [53]:

- Interaction of the vacant orbital of hetero atoms (Back-donation) with d-electrons of surface iron's atom
- Interactions between the aromatic rings (π-electrons) in inhibitors molecules and iron surface atoms (vacant d-orbitals).
- Interactions between the iron surface atoms (vacant d-orbitals) with Unshared electron pairs of hetero-atoms (O and N atoms).

Myrrh is a Natural product that is rich in functional groups (hetero compounds containing oxygen and nitrogen atoms) that enable them to interact modes of steel/ Myrrh interface, Table 1.

Different chemical compounds that present in Myrrh can react with the surface of steel to form metallic-organo complexes $[Fe–Myrrh]^{2+}$, according to the following mechanism (Eq. 5, 6), [54]:

$$Fe \rightarrow Fe^{2+} + 2e \qquad (5)$$

$$Fe^{2+} + Myrrh \rightarrow [Fe - Myrrh]^{2+} \qquad (6)$$

We propose illustration for this phenomenon about the decrease in corrosion resistance with the increase of inhibitor concentration which can be explained on the adsorption as follows (Figure 10):

(i) the molecules of constituents of inhibitor immigrate from HCl solution and adsorb on the steel surface. after that, the surface of metal is partially covered with inhibitor molecules.

(ii) At high concentration, the number of adsorbed molecules is increased. In other words, the surface of metal is completely covered with inhibitor molecules.

(iii) In case of ZnO-NPs, due to the small size of nanoparticles it increases the chance of closing all active places on the metal surface.

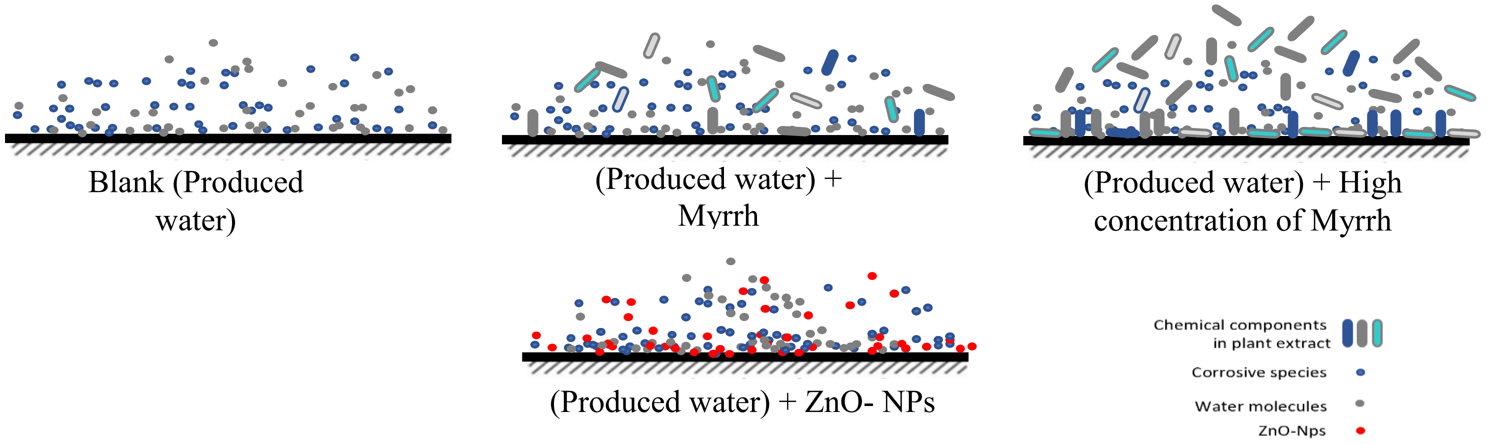
Blank (Produced water)

(Produced water) + Myrrh

(Produced water) + High concentration of Myrrh

(Produced water) + ZnO- NPs

Figure 10. Representation of adsorption mechanism of inhibitor on steel in 0.1 M HCl.

3.6 Scanning Electron Microscopy (SEM) Analysis

During the corrosion process, protective layer formation could be observed in the SEM image. Figure 11 shows the SEM image of steel specimens (a) before immersion, (b) immersed in 1 M HCl, (c) in 1 M HCl with 0.0025 g of *Myrrh,* (d) in 1 M HCl with 0.02 g of *Myrrh*, (e) in 1 M HCl with 0.0025 g of ZnO-NPs, and (f) in 1 M HCl with 0.02 g of ZnO-NPs. Figure 10b illustrates the strong attack of the medium on the steel surface. Moreover, the corrosion products appear too irregular and are arranged layer by layer. Figures 10c and 10d reveal that the steel surface with 0.02 g of *Myrrh* extract experienced much less damage than 0.0025 g of *Myrrh* extract. This can be attributed to the formation of an adsorbed film of extract on the surface. Figures 10e and 10f show the steel surface with 0.02 g of ZnO. The 0.02 g ZnO NP addition caused much less damage compared to that of the 0.0025 g of ZnO-NP addition. From these results, it can be concluded that the ZnO NPs can effectively protect steel samples from a corrosive environment due to their small size.

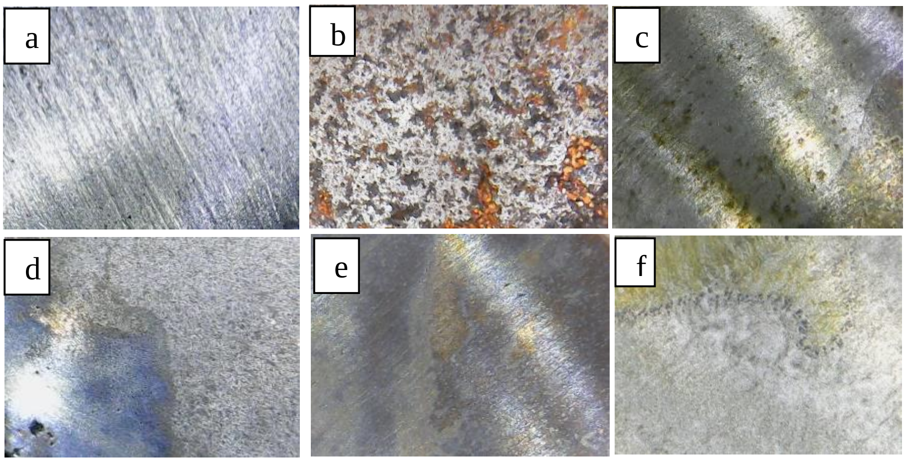

Figure 11. SEM images at 30 °C after immersion for 90 min: (a) blank steel, (b) blank steel + 1.0 M HCl, (c) 0.0025 g of Myrrh solution, (d) 0.02 g of Myrrh solution, (e) 0.0025 g of ZnO/ Myrrh, and (f) 0.02 g of ZnO/ Myrrh. (immersion time:1.5 h)

4. CONCLUSIONS

The following primary conclusions are derived from the present investigation of this research:

1. A green synthesis of ZnO NPs could be obtained by using a natural *Myrrh* extract as an inexpensive capping agent to form highly dispersed ZnO NPs having monodisperse particle sizes.
2. *Myrrh* and ZnO NPs inhibited the corrosion properties of steel in 1 M HCl.
3. Anodic and cathodic reactions could be affected by using both *Myrrh* and/or ZnO NPs due to their adsorption on the steel surface, and thus, these additives functioned as cathodic mixed inhibitors.
4. There was a significant increase in the corrosion inhibition efficiencies of *Myrrh* and ZnO NPs that was in line with their concentrations, and there was good agreement of the obtained values from polarization and EIS measurements.
5. Most importantly, green ZnO NPs can be used as an eco-friendly corrosion inhibitor for steel in a 1.0 M HCl acid solution.

References

1. M. Saeedi, M. Eslamifar, K. Khezri and S. M. Dizaj, *Biomed. Pharmacother.*, 111 (2019) 666.
2. V. Leso, L. Fontana and I. Iavicoli, *Nano Today*, 24 (2019) 10.
3. Z. Ahmadi, *Prog. Org. Coat.*, 132 (2019) 445.
4. J. Roy, S. Chandra and S. Maitra, *Ceram. Int.*, 45 (2019) 19.
5. E. Villena de Francisco and R. M. García-Estepa, *J. Food Eng.*, 238 (2018) 1.
6. F. Adams and C. Barbante, Compr. *Anal. Chem.*, 69 (2015) 125.
7. M. V. Gallegos, F. Aparicio, M. A. Peluso, L. C. Damonte and J. E. Sambeth, *Mater. Res. Bull.*, 103 (2018) 158.
8. A. R. Prasad, P. R. Ammal and A. Joseph, *Mater. Res. Bull.*, 102 (2018) 116.
9. A. Alhadhrami, A. S. A. Almalki, A. A. Adam and M. S. Refat, *Int. J. Electrochem. Sci.*, 13 (2018)

6503.
10. T. Saravanakumar, V. Kavimani, K.S. Prakash and T. Selvaraju, *Prog. Org. Coat.*, 129 (2019) 32.
11. Nikhil, G. Ji and R. Prakash, *J. Mol. Liq.*, 280 (2019) 160.
12. Z. Lin, Y. Wang, D. Zhang and X. Li, *Int. J. Electrochem. Sci.*, 11 (2016) 8512.
13. B. Radwan, A. M. A. Mohamed, A. M. Abdullah and M. A. Al-Maadeed, *Surf. Coat. Tech.*, 289 (2016) 136.
14. E. Velayi and R. Norouzbeigi, *Ceram. Int.*, 45 (2019) 16864.
15. F. E.-T. Heakal and A. E. Elkholy, *J. Mol. Liq.*, 230 (2017) 395.
16. Y. Qian, Y. Li, S. Jungwirth, N. Seely, Y. Fang and X. Shi, *Int. J. Electrochem. Sci.*, 10 (2015) 10756.
17. A. W. Peabody and R. L. Bianchetti (Ed.), Control of Pipeline Corrosion, NACE International, (1967) Houston, TX, United States of America.
18. C. Verma, E. E. Ebenso and M. A. Quraishi, *J. Mol. Liq.*, 233 (2017) 403.
19. N. El Hamdani, R. Fdil, M. Tourabi, C. Jama and F. Bentiss, *Appl. Surf. Sci.*, 357 (2015) 1294.
20. H. Bhandari, V. Choudhary and S. K. Dhawan, *Synth. Met.*, 161 (2011) 753.
21. Y. Fang, B. Suganthan and R. P. Ramasamy, *J. Electroanal. Chem.*, 840 (2019) 74.
22. S. A. Umoren, M. M. Solomon, I. B. Obot and R. K. Suleiman, *J. Ind. Eng. Chem.*, 76 (2019) 91.
23. M. A. Quraishi, A. Singh, V. K. Singh, D. K. Yadav and A. K. Singh, *Mater. Chem. Phys.*, 122 (2010) 114.
24. D. I. Njoku, E. E. Oguzie and Y. Li, *J. Mol. Liq.*, 237 (2017) 247.
25. G. Ji, S. K. Shukla, P. Dwivedi, S. Sundaram and R. Prakash, *Ind. Eng. Chem. Res.,* 50 (2011) 11954.
26. A. K. Satapathy, G. Gunasekaran, S. C. Sahoo, K. Amit and P. V. Rodrigues, *Corros. Sci.*, 51 (2009) 2848.
27. K. P. V. Kumar, M. S. N. Pillai and G. R. Thusnavis, *J. Mater. Sci.*, 46 (2011) 5208.
28. P. Parthipan, J. Narenkumar, P. Elumalai, P. S. Preethi, A. U. R. Nanthini, A. Agrawal and A. Rajasekar, *J. Mol. Liq.*, 240 (2017) 121.
29. P. Mourya, S. Banerjee and M. M. Singh, *Corros. Sci.*, 85 (2014) 352.
30. J. C. da Rocha, J. A. C. P. Gomes and E. D'Elia, *Corros. Sci.,* 52 (2010) 2341.
31. M. M. Fares, A. K. Maayta and M. M. Al-Qudah, *Corros. Sci.*, 60 (2012) 112.
32. M. Abdallah, *Port. Electrochim. Acta*, 22 (2004) 161.
33. H. S. Shukla, N. Haldar and G. Udayabhanu, *J. Corros. Sci. Eng.*, 14 (2011) 1.
34. Z. Salarvand, M. Amirnasr, M. Talebian, K. Raeissi and S. Meghdadi, *Corros. Sci.*, 114 (2017) 133.
35. G. Gece, Corros. Sci., 53 (2011) 3873.
36. A. Rahim, M. Kassim, E. Rocca and J. Steinmetz, *Corros. Eng., Sci. Technol.*, 46 (2011) 425.
37. L. O. Hanuš, T. Řezanka, V. M. Dembitsky and A. Moussaieff, *Biomed. Pap.*, 149 (2005) 3.
38. H. Bentrah, Y. Rahali and A. Chala, *Corros. Sci.*, 82 (2014) 426.
39. M. A. Abu-Dalo, A. A. Othman and N. A. F. Al-Rawashdeh, *Int. J. Electrochem. Sci.*, 7 (2012) 9303.
40. E. Oguzie, Y. Li and F. Wang, *J. Colloid Interface Sci.*, 310 (2007) 90.
41. P. C. Okafor, M. E. Ikpi, I. E. Uwah, E. E. Ebenso, U. J. Ekpe and S. A. Umoren, *Corros. Sci.*, 50 (2008) 2310.
42. S. A Umoren, I. B. Obot, E. E Ebenso, P. C. Okafor, O. Ogbobe and E. E. Oguzie, *Meth. Mat.*, 53 (2006) 277.
43. E. Mincione and C. Iavarone, *Nota I. Chim Ind.,* 54 (1972) 424.
44. A. M. Atta, G. A. El-Mahdy, H. A. Al-Lohedan and S. A. Al-Hussain, *Int. J. Electrochem. Sci.*, 9 (2014) 8446.
45. Q. Qu, L. Li, W. Bai, S. Jiang and Z. Ding, *Corros. Sci.*, 51 (2009) 2423.
46. K. Khaled, *Electrochim. Acta,* 48 (2003) 2493.
47. K. Babić-Samardžija, C. Lupu, N. Hackerman, A. Barron and A. Luttge, *Langmuir*, 21 (2005)

12187.
48. E. McCafferty and N. Hackerman, *J. Electrochem. Soc*., 119 (1972) 146.
49. A. Satapathy, G. Gunasekaran, S. Sahoo, K. Amit and P. Rodrigues, *Corros. Sci*., 51 (2009) 2848.
50. A. M. Al-Turkustani, R. M. Al-Sawat, R. H. Al-Hassani, N. S. Al-Ghamdi, E. M. Al-Harbi, M. A. Al-Gamdi and S. A. Al-Solmi, *J. Chem. Acta*, 2 (2013) 253.
51. V. V. Torres, R. S. Amado, C. F. de Sá, T. L. Fernandez, C. A. Da Silva Riehl, A. G. Torres and E. D'Elia, *Corros. Sci*., 53 (2011) 2385.
52. A. Y. El-Etre, Ahmed H. Tantawy, S. Eid and D. F. Seyam, *Journal of Basic and Environmental Sciences*, 4 (2017) 128.
53. G. Gunasekaran and L. Chauhan, *Electrochim. Acta,* 49 (2004) 4387.
54. F. El-Taib Heakal, A. S. Fouda and M. S. Radwan, *Mater. Chem. Phys*., 125 (2011) 26.